Molecular and Cellular Neuroscience 124 (2023) 103805

Contents lists available at ScienceDirect

Molecular and Cellular Neuroscience

journal homepage: www.elsevier.com/locate/ymcne

# The interaction between intestinal bacterial metabolites and phosphatase and tensin homolog in autism spectrum disorder

Yuanpeng Zheng [a], Naika Prince [a], Christine van Hattem [a], Johan Garssen [a,b], Paula Perez Pardo [a], Aletta D. Kraneveld [a,*]

[a] Division of Pharmacology, Utrecht Institute for Pharmaceutical Sciences, Faculty of Science, Utrecht University, Utrecht, the Netherlands
[b] Global Centre of Excellence Immunology, Danone-Nutricia research, Utrecht, the Netherlands

ARTICLE INFO

*Keywords:*
ASD
PTEN
VPA
*p*CS
4EPS
LPS
Neuroimmune response

ABSTRACT

Intestinal bacteria-associated *para*-cresyl sulfate (*p*CS) and 4-ethylphenyl sulfate (4EPS) are elevated in autism spectrum disorder (ASD). Both metabolites can induce ASD-like behaviors in mice, but the molecular mechanisms are not known. Phosphatase and tensin homolog (PTEN) is a susceptibility gene for ASD. The present study investigated the relation between *p*CS and 4EPS and PTEN in ASD in a valproic acid (VPA)-induced murine ASD model and an *in vitro* LPS-activated microglial model. The VPA-induced intestinal inflammation and compromised permeability in the distal ileum was not associated with changes of PTEN expression and phosphorylation. In contrast, VPA reduced PTEN expression in the hippocampus of mice. *In vitro* results show that *p*CS and 4EPS reduced PTEN expression and derailed innate immune response of BV2 microglial cells. The PTEN inhibitor VO-OHpic did not affect innate immune response of microglial cells. In conclusion, PTEN does not play a role in intestinal inflammation and compromised permeability in VPA-induced murine model for ASD. Although *p*CS and 4EPS reduced PTEN expression in microglial cells, PTEN is not involved in the *p*CS and 4EPS-induced derailed innate immune response of microglial cells. Further studies are needed to investigate the possible involvement of reduced PTEN expression in the ASD brain regarding synapse function and neuronal connectivity.

## 1. Introduction

Autism spectrum disorder (ASD) is a neurodevelopmental disease which core symptoms are impairments in social interaction and communication, deficits in cognitive function as well as the presence of stereotyped behavior (Lord et al., 2018). Recent epidemiological surveys show the worldwide prevalence of ASD is about 1 % (Fombonne et al., 2021). At present, there is no effective treatment targeting ASD detrimental core symptoms (Genovese and Butler, 2020). Although the ASD pathogenesis is not clear, the abnormal changes along the microbiota-gut-brain axis have been reported to be involved (Salim et al., 2021). The involvement of the gut in ASD is also supported by frequently reported gastrointestinal comorbidities, including intestinal inflammation and compromised intestinal barrier (Babinská et al., 2017; Dalton et al., 2014; Kang et al., 2017; Walker et al., 2019).

Children with ASD show changes in gut microbiota and microbiota-associated metabolites (Kang et al., 2020; Kang et al., 2018; Zou et al., 2020). *Para*-cresyl sulfate (*p*CS) and 4-ethylphenyl sulfate (4EPS) are host metabolites derived from two bacterial metabolites, *para*-cresol (*p*-cresol) and 4-ethylphenol, originating from intestinal bacterial fermentation of tyrosine and phenylalanine (Zheng et al., 2021). It has been reported that children diagnosed with ASD show a overgrowth of small intestinal bacteria, indicating that the *p*-cresol- and or 4EP-producing bacteria might be existing in distal ileum (Wang et al., 2018). *p*-Cresol and 4-ethylphenol can be absorbed from the gut and metabolized into *p*CS and 4EPS (Needham et al., 2022; Zheng et al., 2021; Zheng et al., 2022). It has been suggested that 95 % of *p*-cresol and metabolized by the host into *p*CS *via* O-sulfonation, a process that occurs primarily in the liver, and to a smaller extent in colonic epithelial cells (Persico and Napolioni, 2013; Ramakrishna et al., 1991; Rong and Kiang, 2021). In addition, 4-ethylphenol has also been suggested to be sulfated into 4EPS *via* O-sulfonation in the host (Hsiao et al., 2013; Needham et al., 2022). Both *p*CS and 4EPS have been shown to be elevated in urine, feces or serum of children with ASD (Gabriele et al., 2014; Kang et al., 2020; Kang et al., 2018; Needham et al., 2021). We have demonstrated elevated *p*CS in the serum of the valproic acid (VPA)-induced mouse

* Corresponding author.
*E-mail address:* a.d.kraneveld@uu.nl (A.D. Kraneveld).

https://doi.org/10.1016/j.mcn.2022.103805
Received 3 October 2022; Received in revised form 17 November 2022; Accepted 24 December 2022
Available online 30 December 2022
1044-7431/© 2023 The Authors. Published by Elsevier Inc. This is an open access article under the CC BY license (http://creativecommons.org/licenses/by/4.0/).

model for ASD (Zheng et al., 2022). Furthermore, *p*-cresol administration in drinking water causes social behavior deficits and repetitive behavior in mice through remodeling of the gut microbiota (Bermudez-Martin et al., 2021). In addition, intraperitoneal injection of 4EPS into mice induces anxiety-like behavior, a common co-morbidity that may contribute to core ASD symptoms (Hsiao et al., 2013; Needham et al., 2022). Moreover, a clinical trial has recently shown that an oral gastrointestinal (GI)-restricted adsorbent AB-2004 decreases urine *p*CS and 4EPS levels and ameliorates ASD-like behaviors of ASD children without serious side-effects (Stewart Campbell et al., 2022). However, it is unclear yet how these two bacteria-derived metabolites are mechanistically linked with ASD.

Phosphatase and tensin homolog (PTEN) is a well-recognized ASD susceptibility gene and a germline mutation in PTEN has been identified in up to 20 % of children diagnosed with ASD with macrocephaly (Busch et al., 2019; Yehia et al., 2020). Studies in mouse models demonstrate that deletion of PTEN in the cerebral cortex and hippocampus results in increased rates of macrocephaly and abnormal social interactions (Kwon et al., 2006). Moreover, PTEN expression in brain is decreased in *in utero* valproic acid (VPA)-exposed male mice (Mahmood et al., 2018). PTEN inhibition or knockdown attenuates neuroinflammation in mice (Pan et al., 2022; Shen et al., 2021). In contrast, loss-of-function mutation of PTEN in mice upregulates neuroinflammation and enhances microglial phagocytosis (Sarn et al., 2021a; Sarn et al., 2021b). Gut-derived *p*CS and 4EPS are regarded as an important protein-bound uremic toxins associated with chronic kidney disease in human and rodent models (Vanholder et al., 2007; Velenosi et al., 2016). Of interest is the recent finding that in uremic mice a downregulated PTEN expression is associated with peripheral inflammation, indicating the *p*CS can affect PTEN expression (Wei et al., 2022). Our previous study has demonstrated that *p*CS derailed the innate immune response as well as phagocytosis of BV2 microglial cells (Zheng et al., 2022). However, little is known about the interaction between bacteria-derived *p*CS and 4EPS and PTEN in ASD-associated intestinal inflammation and derailed neuroimmune responses in the brain.

The current study aims to investigate the potential relation between PTEN and *p*CS and 4EPS, using *in vivo* and *in vitro* models to unravel the molecular mechanisms involved of how *p*CS and 4EPS contribute to ASD. First, in tissues obtained from *in utero* VPA-exposed male mice the intestinal and brain PTEN phosphorylation and/or expression was assessed. Subsequently BV2 microglial cells were used to investigate whether *p*CS or 4EPS has a direct effect on PTEN expression. Next, the role of PTEN in microglial neuroimmune response and phagocytosis associated with *p*CS and 4EPS was investigated.

## 2. Materials and methods

### 2.1. Mice

As previously described (de Theije et al., 2014), specific pathogen-free BALB/cByJ breeding pairs from Charles River laboratories (Maastricht, the Netherlands) were housed under a 12 h light/dark cycle with free access to water and standard food for laboratory rodents AIN-93 M. All animal procedures were conducted according to governmental guidelines and approved by the Ethical Committee of Animal Research of Utrecht University, Utrecht, the Netherlands (CCD number AVD108002017826). All females were mated until a vaginal plug was detected, indicated as gestational day 0 (G0). On G11, after neural tube closure, pregnant females were treated subcutaneously with 600 mg/kg VPA (Sigma, Zwijndrecht, the Netherlands, VPA: 100 mg/ml) or phosphate buffered saline (PBS). The offspring was weaned on postnatal day 21 (P21). On postnatal day 50, male mice were euthanized by decapitation to collect intestinal tissue and brain tissue (*in utero* PBS-exposed male mice: $n = 3$; *In utero* VPA-exposed male mice: $n = 3$).

### 2.2. Tissue homogenization

Mice hippocampus, prefrontal cortex, cerebellum and olfactory bulbs, and the rest of brain tissue was also isolated. These brain regions were homogenised at 4 °C using STET buffer without detergents (50 mM Tris, pH 7.5, 150 mM NaCl, 2 mM EDTA, Proteinase Inhibitor Cocktail (1:200, P8340, Sigma), 5 μM GI254023X (SML0789, Sigma), 10 mM 1,10-Phenanthroline (131,377, Sigma)) (Brummer et al., 2018). After centrifugation at 12,000*g*, 15 min, 4 °C, brain tissue lysate was further lysed on ice for 30 min with RIPA buffer (20,188, Sigma) containing 1 % TritonX-100 detergent, Proteinase Inhibitor Cocktail (1:200), 5 μM GI254023X and 10 mM 1,10-Phenanthroline, next it was centrifugated again at 12,000 g, 15 min, 4 °C to collect the supernatant for Western blotting (WB) analysis after protein quantification with Pierce™ BCA Protein Assay Kit (23,225, Thermo Scientific, Vantaa, Finland).

For intestinal tissues, the distal ileum was homogenised with Precellys Control Device (5500 rpm, 2*20s), then samples were put in beads-containing homogenization tubes (P000918-LYSK0-A, Precellys) with RIPA lysis buffer containing Proteinase inhibitor (1:200), phosphatase inhibitor (1:50, ab 201,112, Abcam), 5 μM GI254023X and 10 mM 1,10-Phenanthroline. After 20 min lysing on ice, the homogenised solution was centrifuged (12,000 *g*, 4 °C, 15 min). Next, supernatant was used for protein quantification using Pierce™ BCA Protein Assay Kit. Then all supernatants were denatured at 95 °C for 5 min in 4× Laemmli Sample Buffer (1,610,747, Bio-Rad, USA) containing 50 mM Dithiothreitol (1,610,611, Bio-Rad, USA).

### 2.3. Cell culture and treatments

As previously described (Bocchini et al., 1992), BV2 cells were cultured at 37 °C and 5 % CO2 in the medium (Dulbecco's modified eagle medium (DMEM) (Gibco, NY, USA), 10 % Fetal bovine serum (Gibco, NY, USA) and 1 % penicillin/streptomycin (Gibco, NY, USA)). BV2 cells were used to investigate possible effects of *p*CS (A8895, APExBIO, USA) or 4EPS (TRC-E925865, Hölzel Diagnostika, the Netherlands) on cell viability, on PTEN, Inducible nitric oxide synthase (iNOS) and Cyclooxygenase-2 (COX-2) expression, on the inflammatory cytokines TNF-α and IL-6 as well as on microglial phagocytosis.

### 2.4. BV2 microglial cell viability

To investigate the effect of 4EPS on cell viability, 5000 BV2 cells/well were incubated with 4EPS (concentration range: 0.1–400 μM) for 24 h. After 24 h, 50 μl medium of each well was transferred into new 96-well plate and the content of lactate dehydrogenase (LDH) in medium was measured by Cytotoxicity Detection KitPLUS (LDH) (4,744,926,001, Sigma) according to the manufacturer's instructions. Meanwhile, the medium left was removed and 100 μl DMEM containing 0.5 mg/ml MTT (M2128, Sigma) was added to the cells for 4 h of incubation at 37 °C under 5 % $CO_2$. 200 μl Dimethyl sulfoxide (DMSO) was added into each well after the DMEM was removed. Finally, optical density values were measured at wavelength of 570 nm. In all viability experiments, 1 μM and 10 μM Rotenone dissolved in DMSO was used as positive control (Avallone et al., 2020; Günaydin et al., 2021).

### 2.5. PTEN expression and inflammatory response in BV2 microglial cells

To study the effect of *p*CS and 4EPS on the release of TNF-α and IL-6 or on the expression of PTEN, COX-2 and iNOS in cells, 5000 BV2 cells/well were seeded in a 96-well plate (3599, Corning, NY, USA) or 50,000 BV2 cells/well in a 12-well plate (3512, Corning, NY, USA), respectively. On the following day, the cells were incubated with *p*CS and 4EPS concentrations in the presence or absence of 1000 ng/ml LPS stimulation (L3024, Sigma). After 24 h of incubation, the medium in 96-well plate was collected for measurements of TNF-α and IL-6 by enzyme-linked immunosorbent assay (ELISA). The BV2 cells in 12-well plate

were lysed in RIPA lysis buffer containing Proteinase inhibitor (1:200), 5 μM GI254023X and 10 mM 1,10-Phenanthroline for WB analysis. For experiments to study the effect of PTEN inhibition on the inflammatory response of microglial cells, 5000 BV2 cells/well were seeded into 96-well plate overnight. On the following day, BV2 cells were incubated with a potent PTEN inhibitor VO-OHpic trihydrate (V8639, Sigma) (Mak et al., 2010) for 24 h in the absence or presence of 1000 ng/ml LPS stimulation. Finally, the medium was used for measurements of inflammatory cytokines TNF-α and IL-6 using ELISA.

### 2.6. Phagocytosis activity assay

50,000 BV2 cells/well were seeded into 96-well plate (3599, Corning, NY, USA). To assess the effect of 4EPS on phagocytosis, BV2 cells were immediately incubated with 4EPS concentrations (0.1, 1, 10 and 100 (μM)) for 24 h in the presence or absence of 1000 ng/ml LPS stimulation. To study the effect of PTEN inhibition on constitutive and LPS-stimulated microglial phagocytosis, BV2 cells were immediately incubated with VO-OHpic trihydrate concentrations (50, 100, 200 and 400 (nM)) for 24 h with or without 1000 ng/ml LPS. Next the phagocytic effect was measured with Vybrant™ Phagocytosis Assay Kit (V6694, Thermo Scientific) according to manufacturer's instructions. Briefly, the medium was discarded completely after 24 h incubation, and cells were incubated with K-12 strain bioParticles for 2 h at 37 °C, followed by Trypan Blue solution incubation for 1 min. Finally, the fluoresce intensity of BV2 cells was measured using ~480 nm excitation, ~520 nm emission.

### 2.7. ELISA

TNF-α and IL-6 concentrations after *p*CS treatment (5, 10, 50 and 150 (μM)) in the medium of BV2 cells were measured by mouse TNF-α ELISA kit (88–7324-88, Invitrogen, USA) and mouse IL-6 ELISA kit (88–7064-88, Invitrogen, USA) according to manufacturer's instructions. TNF-α and IL-6 concentrations with 4EPS (0.1, 1, 10 and 100 (μM)) or VO-OHpic trihydrate (50, 100, 200 and 400 (nM)) treatment in the medium of BV2 cells were measured by mouse TNF-α ELISA kit (430,901, BioLegend, USA) and mouse IL-6 ELISA kit (431,301, BioLegend, USA) according to manufacturer's instructions. IL-6 concentrations in medium after exposure to 4EPS treatment (0.1, 1 and 10 μM) were under the detection limit that were set as '0'.

### 2.8. Immunoblotting mouse tissue and BV2 microglial cells

As described previously (Brummer et al., 2018; Pigoni et al., 2020), 10–30 μg of protein was loaded and separated on 4–15 % gradient precast polyacrylamide gels (5,671,084, Bio-Rad, USA). Next, proteins were transferred to PVDF membranes (1,704,157, Bio-Rad, USA) with Trans-Blot Turbo Transfer System. The membranes were blocked in 5 % skim milk-PBST for 1 h and then incubated with the primary antibody overnight at 4 °C. The membranes were washed with PBST buffer and incubated with anti-rabbit (1:3000, Dako, P0448, USA) or anti-mouse (1:3000, Dako, P0260, USA) secondary antibodies for 1 h at room temperature. After washing, the membranes were exposed to Clarity Western ECL Blotting Substrate (1,705,060, Bio-Rad Laboratories, Hercules, CA, USA), and were imaged using the ChemiDoc MP Imaging System (Bio-Rad Laboratories, Hercules, CA, USA) to detect bands. Image J software (version 1.52v, National Institutes of Health, USA) was employed to quantify the density of the bands. The following primary antibodies were used: PTEN primary antibody (1:1000, 9556S, CST), phosphorylated(p)-PTEN (Ser380/Thr382/383) primary antibody (1:1000, 9549S, CST), COX-2 primary antibody (1:1000, 12282S, CST), iNOS primary antibody (1:500, MAB9502, Novus Biologicals), E-cadherin primary antibody (1:1000, 610,182, BD Science), and β-ACTIN primary antibody (1:3000, MA5–15739, Invitrogen, USA) or Calnexin primary antibody (1:3500, PA5–34754, Invitrogen, USA) as loading control.

### 2.9. Statistics

All data analyses and statistics were performed using GraphPad Prism (version 9.1.1; GraphPad software, La Jolla, CA, USA). The *in vivo* results were analyzed by two-tailed Student's test. Two-tailed Pearson correlation was used for correlation analysis of E-cadherin and iNOS expression in the distal ileum of mice. For multiple comparisons of the *in vitro* data, one-way ANOVA was used, followed by Dunnett's multiple comparisons as post-hoc test. All data are shown as mean ± SEM or mean ± SD; $P < 0.05$ is considered to be statistically significant.

## 3. Results

### 3.1. Valproic acid-induced murine model for ASD

#### 3.1.1. PTEN expression and PTEN phosphorylation did not change in the distal ileum of male mice after in utero exposure to VPA

Previous studies have shown intestinal inflammation in VPA-induced murine model of ASD (de Theije et al., 2014). COX-2 expression was significantly increased to six folds in the distal ileum of *in utero* VPA-exposed mice compared to control mice, indicating a VPA-induced intestinal inflammatory response (Fig. 1A & B). Furthermore, membrane-bound E-cadherin was significantly decreased in the distal ileum of *in utero* VPA-exposed mice compared to control mice (Fig. 1C & D). The decreased membrane-bound E-cadherin leads to increased C-terminal fragment of E-cadherin levels (CT E-cadherin). Indeed, we found a trend of increased CT E-cadherin (Fig. 1E $P = 0.083$) and significantly increased ratio of CT E-cadherin to membrane-bound E-cadherin (Fig. 1F). It has been shown that iNOS co-localizes with adhesive protein E-cadherin, indicating E-cadherin might regulate iNOS expression or *vice versa* (Frank and Hostetter, 2007; Glynne et al., 2002; Terciolo et al., 2017). The decreased E-cadherin expression was associated with a decreased iNOS expression in the distal ileum of *in utero* VPA-exposed mice compared to control mice (Fig. 1G & H ($P = 0.056$). Furthermore, the Pearson correlation analysis shows a strong correlation between E-cadherin expression and iNOS expression ($r = 0.87$, $P = 0.024$, Fig. 1I). Next, we assessed whether PTEN expression or PTEN phosphorylation is changed in the inflamed distal ileum of *in utero* VPA-exposed male mice. As shown in Fig. 1K & M, both PTEN and phosphorylated PTEN expression show no differences between *in utero* VPA-exposed and control mice.

#### 3.1.2. In utero exposure to VPA attenuated PTEN expression in hippocampus, without effects in other brain regions in male mice

PTEN expression significantly decreased in the hippocampus of *in utero* VPA-exposed male mice compared to control mice (Fig. 2A & B). In contrast, PTEN expression of *in utero* VPA-exposed mice was not significantly changed compared to control mice in the prefrontal cortex (supplementary fig. 1A & B), cerebellum (supplementary fig. 1C & D), olfactory bulb (supplementary fig. 1E & F), and in the rest of other mice brain regions (supplementary fig. 1G & H).

These *in vivo* results indicate that *in utero* exposure to VPA down regulates PTEN expression in the hippocampus but not affect PTEN expression in the distal ileum in male mice. Elevated levels of the intestinal bacteria-derived metabolite *p*CS in serum of *in utero* VPA-exposed male mice has been shown in previous studies (Zheng et al., 2022). In the present study, we hypothesize that the intestinal bacteria-derived *p*CS and 4EPS induce ASD-like behaviors *via* affecting PTEN expression of microglial cells in the brain in this murine model for ASD. Therefore, the direct effect of *p*CS and 4EPS on PTEN expression in BV2 microglial cells and the possible association with neuro-immune responses and microglial phagocytosis function are investigated.

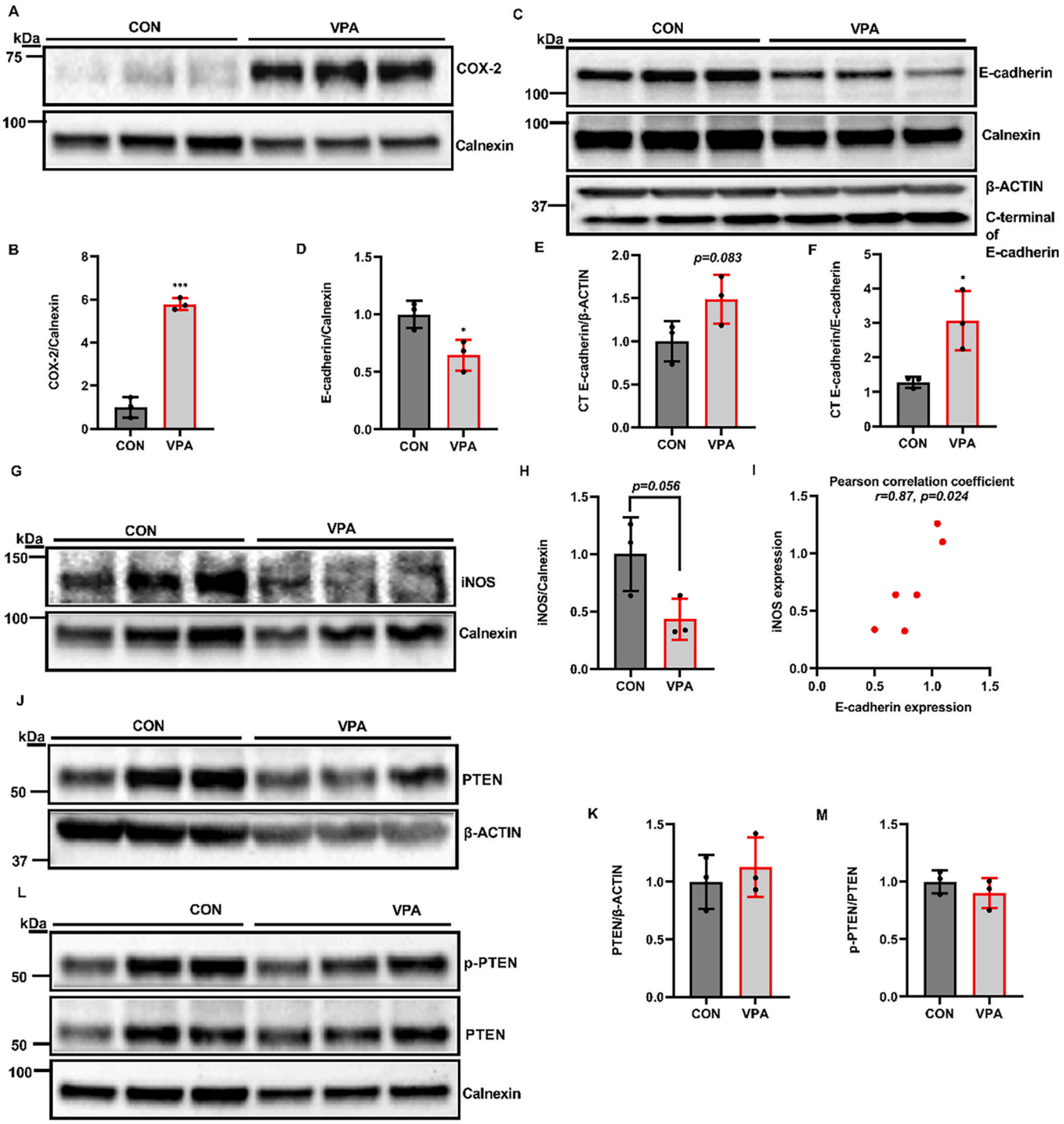


**Fig. 1.** The effects of *in utero* VPA-exposure on COX-2, iNOS, E-cadherin, as well as PTEN expression and PTEN phosphorylation in the distal ileum of male mice. (A) Immunoblots of COX-2. (B) The quantification of COX-2 expression. (C) The immunoblots of membrane-associated E-cadherin and C-terminal (CT) fragment of E-cadherin. (D, E) The quantification of E-cadherin and CT E-cadherin expression. (F) The ratio of CT E-cadherin to E-cadherin. (G) The immunoblots of iNOS. (H) The quantification of iNOS expression. (I) Pearson correlation analysis of E-cadherin and iNOS. (J) The immunoblots of PTEN. (K) The quantification of PTEN expression. (L)The immunoblots of phosphorylated PTEN (p-PTEN). (M) The quantification of p-PTEN expression. Calnexin or β-ACTIN were used as loading control. $n = 3$ for *in utero* PBS- or VPA-exposed male mice. Results are shown as mean ± SD. $^{*}P < 0.05$, $^{***}P < 0.001$.

### 3.2. Inflammatory response of microglial cells

#### 3.2.1. pCS and 4EPS attenuated constitutive and LPS-activated PTEN expression in BV2 microglial cells

Previously we demonstrated that 24-h exposure of BV2 microglial cells up to a concentration of 500 μM *p*CS did not affect their viability (Zheng et al., 2022). In the present study, we show that 4EPS up to a concentration of 400 μM did also not have toxic effects on BV2 microglial cells after 24 h incubation using two cell viability assays (MTT and LDH) (supplementary fig. 2).

The direct effects of *p*CS and 4EPS on PTEN expression in BV2 microglial cells were assessed. As shown in Fig. 3A-D, 5 to 150 μM *p*CS,

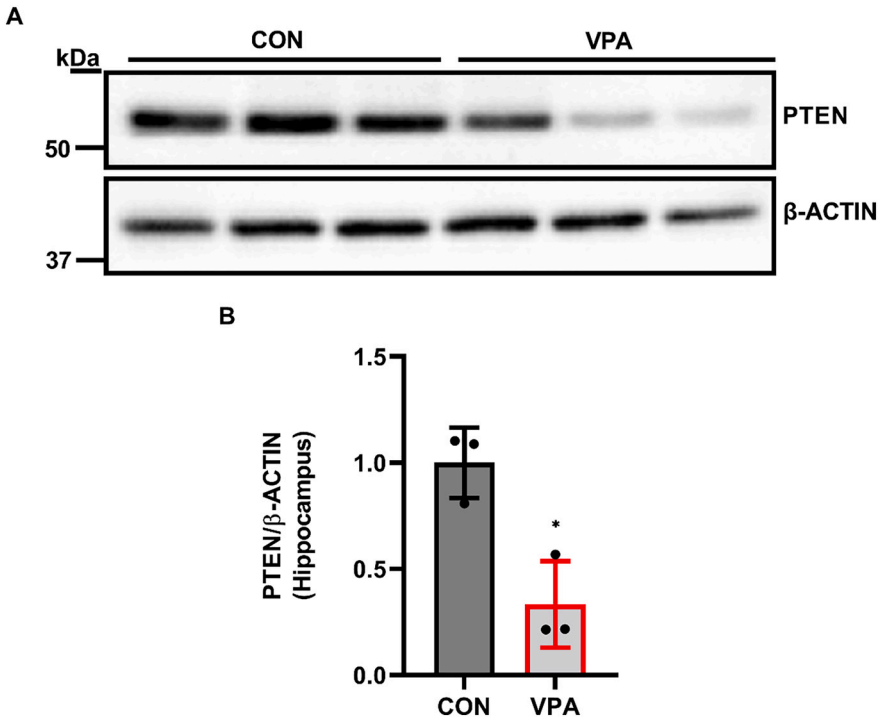


**Fig. 2.** *In utero* VPA-exposure to male mice demonstrated a decreased PTEN expression in hippocampus. (A) The immunoblots of hippocampal PTEN. (B) The quantification of hippocampal PTEN expression. β-ACTIN was used as loading control. $n = 3$ for *in utero* PBS- or VPA-exposed male mice. Results are expressed as mean ± SD. $^{*}P < 0.05$.

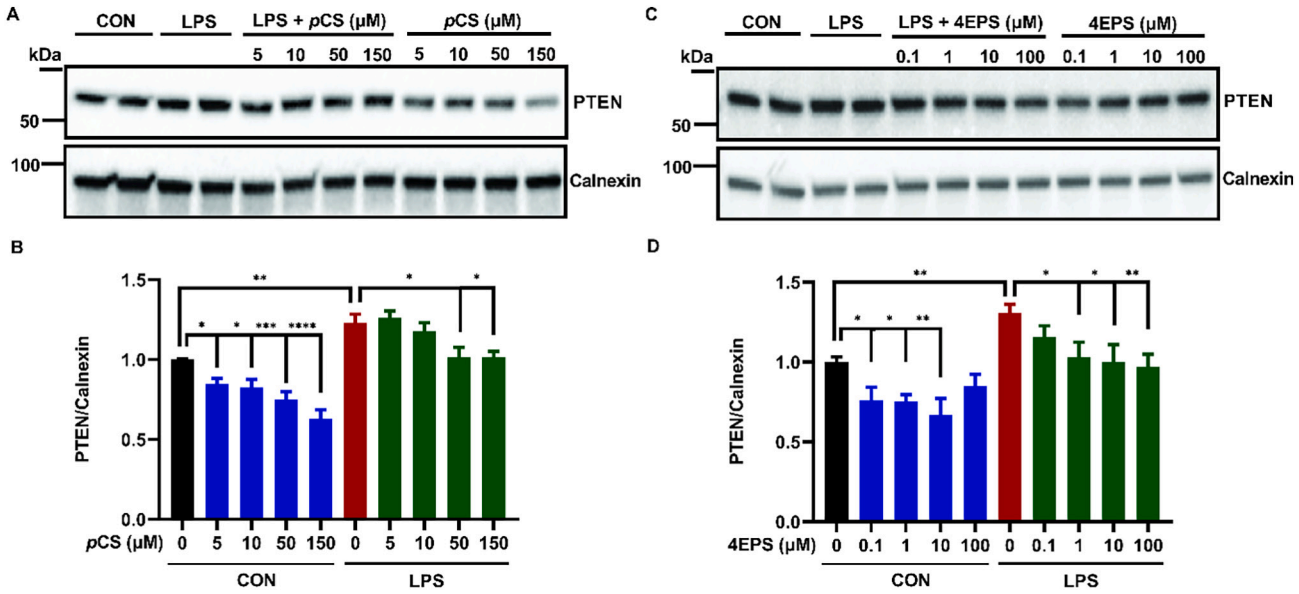


**Fig. 3.** The effects of *p*CS or 4EPS on constitutive and LPS-activated PTEN expression in BV2 microglial cells. BV2 microglial cells were incubated with *p*CS or 4EPS for 24 h in the absence or presence of 1000 ng/ml LPS. Cell lysate was collected for WB analysis. (A) The representative immunoblots of PTEN with *p*CS treatment. (B) The quantification of PTEN expression of microglial cells exposed to *p*CS ($n = 4$ from 4 independent experiments). (C) The representative immunoblots of PTEN with 4EPS treatment. (D) The quantification of PTEN expression of microglial cells exposed to 4EPS treatment ($n = 6$ from 6 independent experiments). Calnexin was used as loading control. Black: control; red: control LPS-activated microglial cells; blue: constitutive active microglial cells; green: LPS-activated microglial cells. Results are shown as mean ± SEM. $^{*}P < 0.05$, $^{**}P < 0.01$, $^{***}P < 0.001$, $^{****}P < 0.0001$.

and 0.1 to 10 μM 4EPS significantly decreased constitutive PTEN expression dose-dependently compared to vehicle-incubated cells. In parallel, LPS stimulation significantly increased PTEN expression compared to control cells. Furthermore, *p*CS (at a concentration of 5 and 150 μM) and 4EPS (at a concentration of 1, 10 and 100 μM) significantly attenuated the LPS-induced increase of PTEN expression in BV2 microglial cells (Fig. 3A & B and Fig. 3C & D, respectively). These results suggest that these two bacteria-derived metabolites can directly reduce PTEN expression of microglial cells constitutively and under inflammation.

*3.2.2. pCS and 4EPS attenuated LPS-induced TNF-α and IL-6 release by BV2 microglia cells, which was not regulated by PTEN*

As shown previously (Bao et al., 2019; Yang et al., 2020; Zheng et al., 2022), LPS stimulation significantly increased TNF-α and IL-6 release from microglial cells (Fig. 4A-F). Confirming previous results, *p*CS inhibited the LPS-induced TNF-α and IL-6 release from microglial cells (Fig. 4A & B). Similar inhibitory effects were found for 4EPS (Fig. 4C & D). In addition, like *p*CS (Zheng et al., 2022), 4EPS treatment reduced constitutive release of TNF-α and IL-6 from microglia (Fig. 4C & D).

Next, the effect of a PTEN inhibitor VO-OHpic (50, 100, 200 and 400 nM) on the constitutive and LPS-induced release of TNF-α and IL-6 by microglial cells was investigated (Mak et al., 2010). As Fig. 4E & F show, VO-OHpic neither affected the constitutive nor the LPS-induced releases of TNF-α and IL-6 by microglial cells, indicating that PTEN is not involved in the constitutive or LPS-induced release of TNF-α and IL-6 by microglial cells. In summary, these results indicate that the *p*CS and 4EPS-induced inhibition of PTEN expression is not involved in the *p*CS and 4EPS-induced effects on constitutive and LPS-induced release of TNF-α and IL-6 of microglial cells.

In addition to the inflammatory cytokines TNF-α and IL-6, iNOS and COX-2 play important role in neuroinflammatory response in brain (Aïd and Bosetti, 2011; Sonar and Lal, 2019). It has been shown previously that LPS stimulation upregulates the protein expressions of these two inflammatory targets in BV2 microglial cells (Nam et al., 2018; Yang

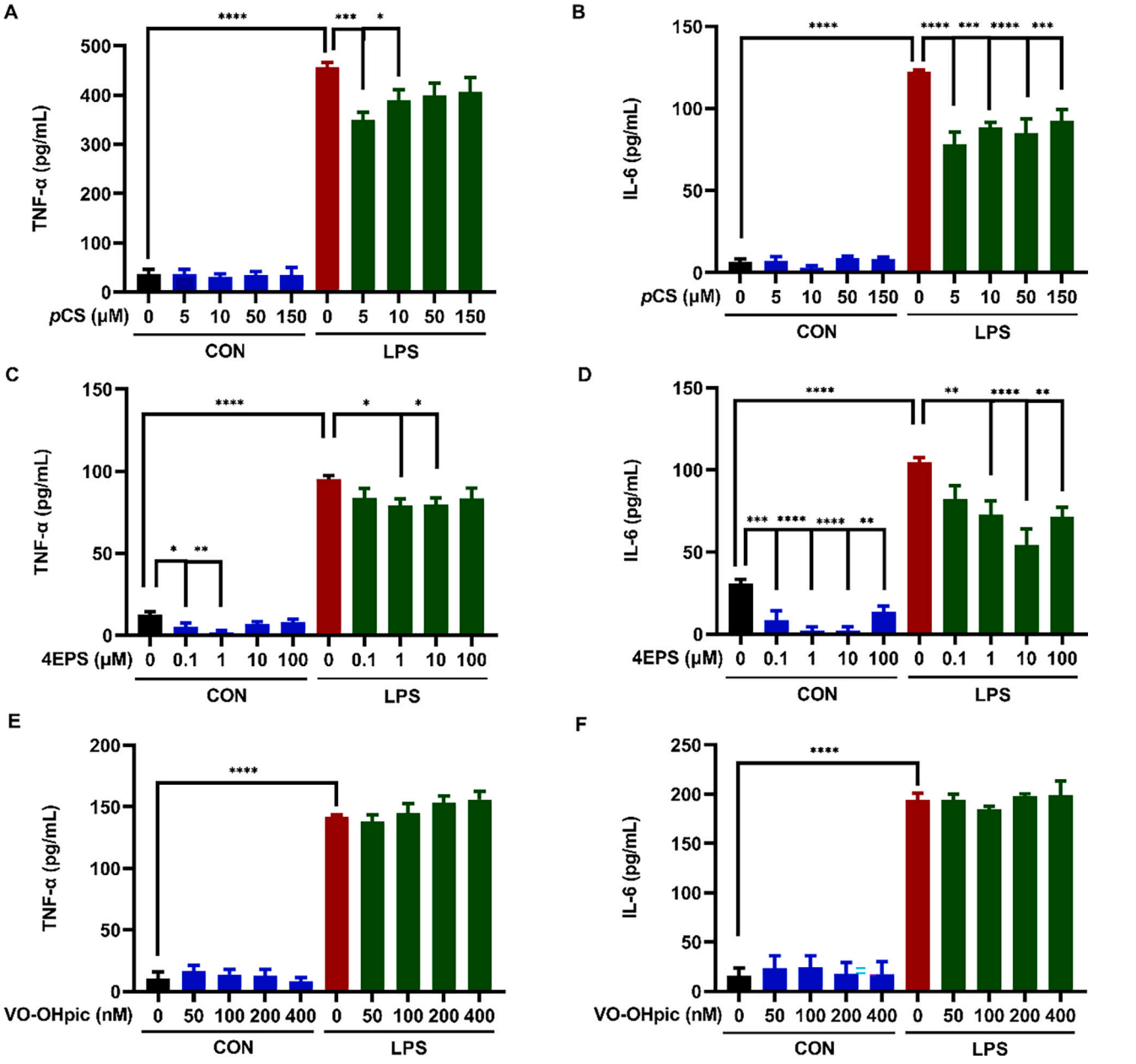


**Fig. 4.** The effects of *p*CS, 4EPS and PTEN inhibitor VO-OHpic on TNF-α and IL-6 release from BV2 microglial cells. BV2 microglial cells were seeded with a density of 5000 each well into 96-well plate, then exposed to *p*CS, 4EPS, and VO-OHpic for 24 h in the absence or presence of 1000 ng/ml LPS, respectively, culture medium was collected for ELISA measurements. (A, B) The TNF-α and IL-6 concentration in medium after *p*CS treatment. ($n = 6$ and 4 from 6 and 4 independent experiments respectively). (C, D) The TNF-α and IL-6 concentration in medium after 4EPS treatment. ($n = 3$ and 4 from 3 and 4 independent experiments respectively). (E, F) The TNF-α and IL-6 concentration in medium after VO-OHpic treatment. ($n = 4$ and 3 from 4 and 3 independent experiments respectively). Black: control; red: control LPS-activated microglial cells; blue: constitutive active microglial cells; green: LPS-activated microglial cells. Results are shown as mean ± SEM. *$P < 0.05$, **$P < 0.01$, ***$P < 0.001$, ****$P < 0.0001$.

et al., 2020), but there is little known about the effect of *p*CS and 4EPS on the expression of iNOS and COX-2. Therefore, the same *in vitro* model of BV2 microglial cells was further used to investigate the effect of *p*CS and 4EPS on iNOS and COX-2 expression in BV2 microglia.

### 3.2.3. *pCS and 4EPS inhibited LPS-activated iNOS expression in BV2 microglial cells*

iNOS is an inflammation-induced protein and is barely constitutively expressed in microglial cells (Nakazawa et al., 2017; Zamora et al., 2000). As shown in Fig. 5A-D, LPS stimulation strongly increased iNOS expression in microglial cells compared to control, which can be attenuated by co-incubation with *p*CS (50 μM) and 4EPS (10 and 100 μM), respectively. These results further support that *p*CS and 4EPS can attenuate LPS-induced neuroinflammation in microglial cells.

### 3.2.4. *pCS and 4EPS were unable to affect LPS-activated COX-2 expression. 4EPS alone increased constitutive COX-2 expression in BV2 microglial cells*

LPS stimulation significantly increased COX-2 expression in microglial cells (Fig. 6A-D). Neither *p*CS nor 4EPS treatment affected LPS-induced COX-2 expression. To better detect COX-2 bands without LPS stimulation, microglial cell lysates after *p*CS or 4EPS exposures were exposed longer separately. As shown in Fig. 6E & F, no clear difference was observed in relation to the constitutive COX-2 expression in microglial cells exposed to 5, 10, 50 or 150 μM *p*CS compared to control. In contrast, 1, 10 and 100 μM 4EPS significantly increased COX-2 expression in microglial cells compared to control without LPS stimulation (Fig. 6G & H). These results indicate that the bacterial metabolites *p*CS and 4EPS do not affect LPS-activated COX-2 expression, but 4EPS can increase constitutive COX-2 expression of microglial cells.

### 3.2.5. *4EPS or PTEN inhibitor VO-OHpic did not affect constitutive and LPS-activated microglial phagocytosis activity*

Previous results have shown that *p*CS treatment attenuated constitutive phagocytosis activity in microglial cells without affecting LPS-induced microglial enhanced phagocytosis activity (Zheng et al., 2022). In the present study, the effects of 4EPS or PTEN inhibitor VO-OHpic on microglial phagocytosis were studied. Confirming the previous finding, LPS stimulation significantly increases microglial phagocytosis activity (Fig. 7A & B). As shown in Fig. 7A, 4EPS treatments from 0.1 μM to 100 μM did not affect constitutive or LPS-induced microglial phagocytosis. In addition, 50 nM to 400 nM VO-OHpic also did not affect microglial phagocytic activity with or without LPS stimulation (Fig. 7B), indicating that 4EPS and PTEN do not play a role in microglial phagocytosis.

## 4. Discussion

The present study investigated the relation between two bacteria-derived metabolites, *p*CS and 4EPS, and PTEN in the pathogenesis of ASD along the gut-brain axis using an *in utero* VPA-induced murine model of ASD and an *in vitro* LPS-activated microglial neuroinflammation model. In this current study, it was demonstrated that PTEN expression was not changed in the distal ileum of *in utero* VPA-exposed male mice, which is associated with enhanced levels of serum *p*CS. The observation that PTEN expression is reduced in the brain of *in utero* VPA-exposed male mice directed us to investigate the role of PTEN regarding the effects of *p*CS and 4EPS on microglial cell function *in vitro*. The decreased PTEN expression in the brain in the murine model for ASD is mirrored by *p*CS and 4EPS-induced decrease in PTEN in microglial cells. However, this *p*CS and 4EPS-induced reduction in PTEN expression does not appear to play a role in the bacteria-derived metabolite-induced derailed innate immune and phagocytotic response of microglial cells.

Increased intestinal permeability and intestinal inflammation frequently occur in children with ASD as well as in rodent models for ASD (Babinská et al., 2017; Kang et al., 2017; Ristori et al., 2019; Walker et al., 2019). Seike et al. have previously shown that *Clostridioides perfringens* Delta-toxin causes increased intestinal permeability or epithilial permeability through decreaseing E-cadherin expression in mouse ileal loop or epithelial Caco-2 cells, respectively (Seike et al., 2019; Seike et al., 2018). In the present study, it was demonstrated that *in utero* exposure to VPA decreased E-cadherin expression in distal ileum, indicative of increased intestinal permeability, which is also supported

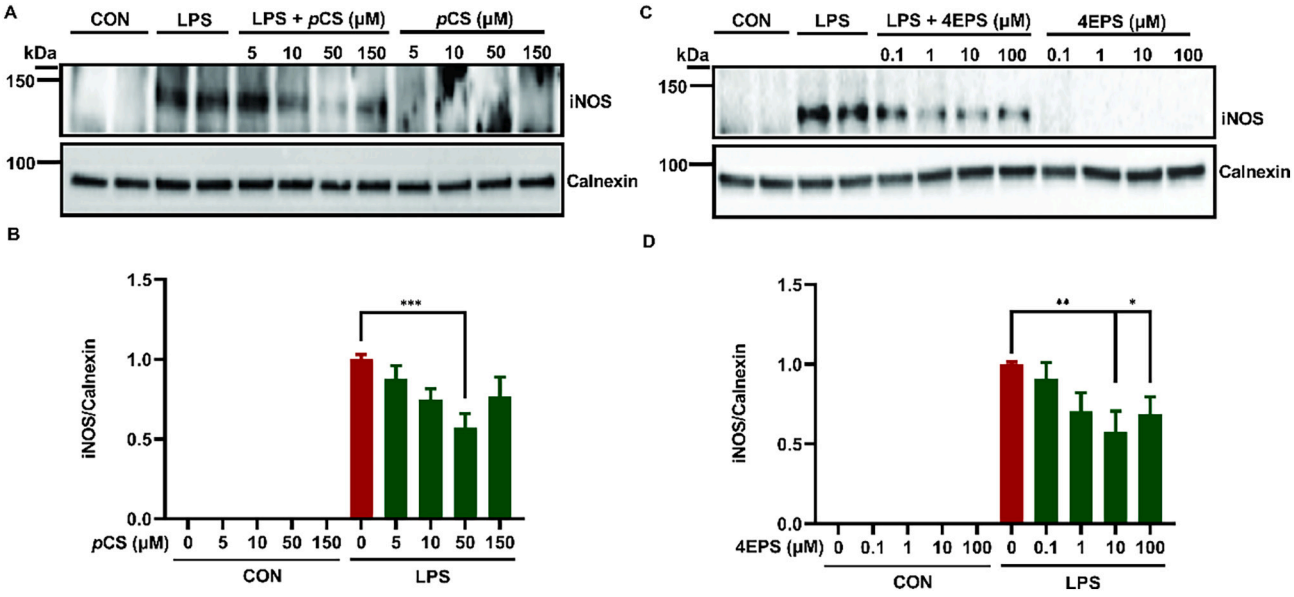


**Fig. 5.** The effects of *p*CS or 4EPS on iNOS expression in BV2 microglial cells. BV2 microglial cells were seeded with a density of 50,000 per well into 12-well plate and then incubated with *p*CS or 4EPS for 24 h in the absence or presence of 1000 ng/ml LPS. Cell lysate was collected for WB analysis. (A) The representative immunoblots of iNOS with *p*CS treatment. (B) The quantification of iNOS expression after *p*CS treatment ($n = 4$ from 4 independent experiments). (C) The representative immunoblots of iNOS with 4EPS treatment. (D) The quantification of iNOS expression after 4EPS treatment (n = 4 from 4 independent experiments). Calnexin was used as loading control. Red: LPS-control; green: LPS-activated microglial cells. Results are shown as mean ± SEM. *$P < 0.05$, **$P < 0.01$, ***$P < 0.001$.

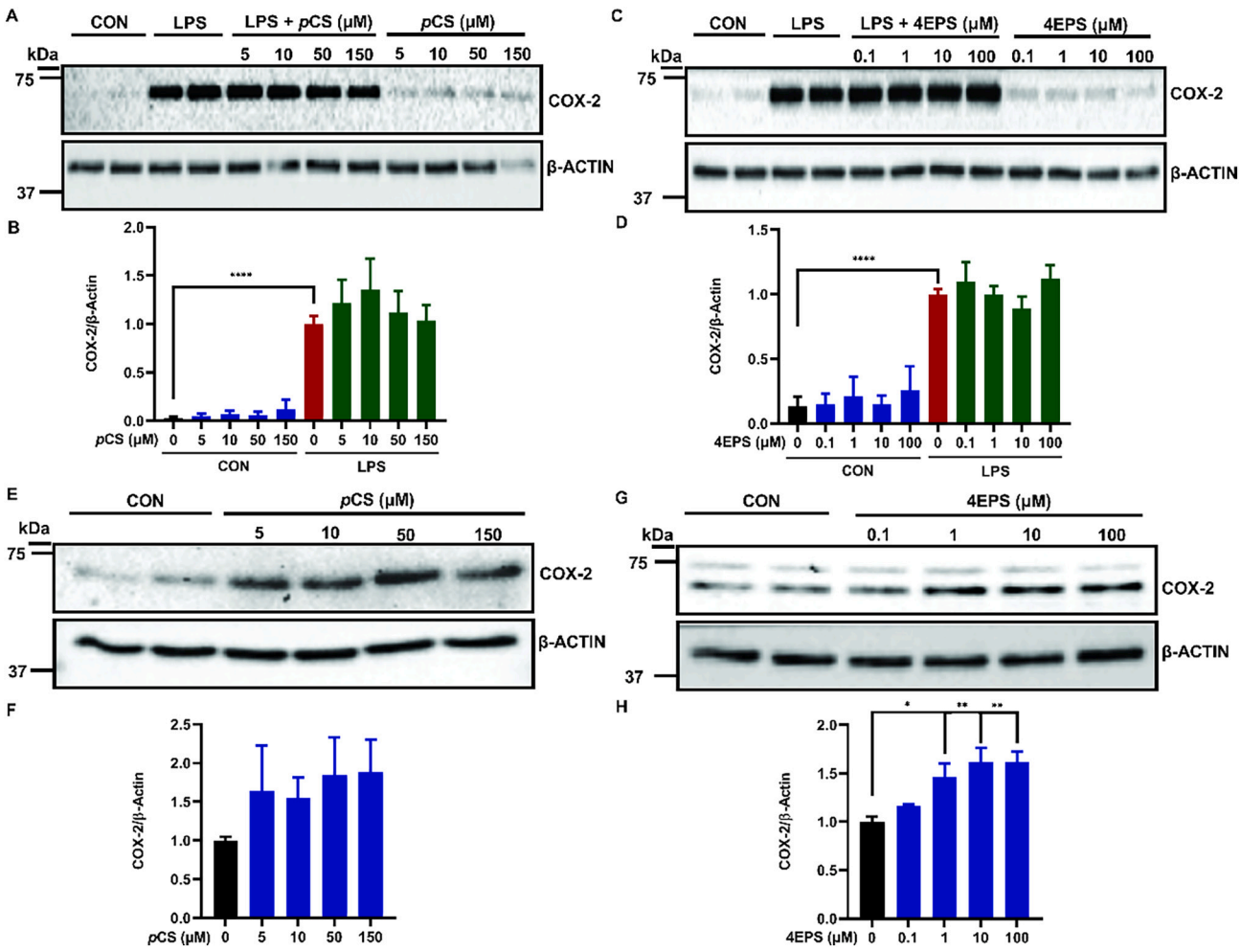


**Fig. 6.** The effects of *p*CS or 4EPS on COX-2 expression in BV2 microglial cells. BV2 microglial cells were seeded with a density of 50,000 per well into 12-well plate and then incubated with *p*CS or 4EPS for 24 h in the absence or presence of 1000 ng/ml LPS. Next cell lysate was collected for WB analysis. (A) The representative immunoblots of COX-2 with *p*CS treatment. (B) The quantification of COX-2 expresison after *p*CS treatment ($n = 4$ from 4 independent experiments). (C) The representative immunoblots of COX-2 with 4EPS treatment. (D) The quantification expression of COX-2 after 4EPS treatment (n = 4 from 4 independent experiments). (E) The representative immunoblots of COX-2 with *p*CS treatment in the absence of LPS stimulation. (F) The quantification of COX-2 expression after *p*CS treatment in the absence of LPS stimulation. (n = 4 from 4 independent experiments). (G) The representative immunoblots of COX-2 with 4EPS treatment in the absence of LPS stimulation. (H) The quantification of COX-2 expression after 4EPS treatment in the absence of LPS stimulation. ($n = 3$ from 3 independent experiments). β-ACTIN was used as loading control. Black: control; red: control LPS-activated microglial cells; blue: constitutive active microglial cells; green: LPS-activated microglial cells. Results are shown as mean ± SEM. *$P < 0.05$, **$P < 0.01$, ****$P < 0.0001$.

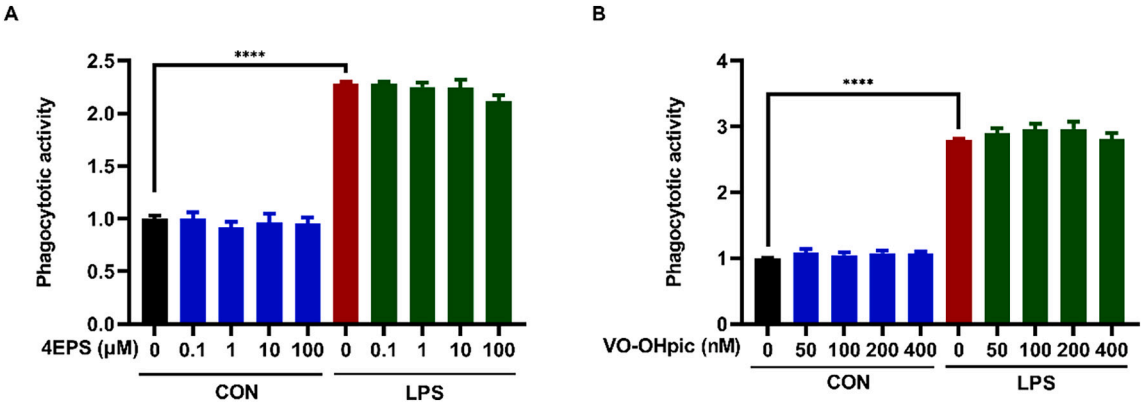


**Fig. 7.** The effects of 4EPS and PTEN inhibitor on microglial phagocytosis function in BV2 cells. BV2 cells were incubated with 4EPS or VO-OHpic for 24 h in the absence or presence of 1000 ng/ml LPS respectively. (A). The effect of 4EPS treatment on BV2 microglial phagocytosis activity ($n = 4$ from 4 independent experiments). (B). The effect of VO-OHpic treatment on BV2 microglial phagocytosis activity ($n = 5$ from 5 independent experiments). Black: control; red: control LPS-activated microglial cells; blue: constitutive active microglial cells; green: LPS-activated microglial cells. Results are shown as mean ± SEM. ****$P < 0.0001$.

by the enhanced intestinal permeability reported *in utero* VPA-exposed rats (Wang et al., 2020). Glynne et al. have shown that E-cadherin co-localizes with epithelial iNOS (Glynne et al., 2002). In addition, decreased iNOS activity or expression increases intestinal permeability through attenuating the expression of tight junctional proteins in mouse ileal tissue (Han et al., 2004). These previous studies support the decreased iNOS expression that was observed in the distal ileum of *in utero* VPA-exposed male mice in the current study. In addition, it was demonstrated that the distal ileum of *in utero* VPA-exposed male mice was inflamed as indicated by enhanced COX-2 protein expression that is an indicator of intestinal and epithelial inflammation (Golden et al., 2020; Wang and Dubois, 2010; Wu et al., 2019), which is supported by previous study showing the presence of inflammation in small intestine of in *in utero* VPA exposed mice (de Theije et al., 2014). Next, PTEN and p-PTEN expression in the same ileal tissue were examined. We found that *in utero* exposure to VPA did not to affect (p-)PTEN expression in ileum. These data suggest that PTEN is not relevant for the compromised barrier and intestinal inflammation in the ileum of *in utero* VPA-exposed male mice.

Both *p*CS and 4EPS are found to be elevated in urine, feces or serum of children diagnosed with ASD and can induce ASD-like behaviors in mice (Bermudez-Martin et al., 2021; Gabriele et al., 2014; Hsiao et al., 2013; Kang et al., 2020; Kang et al., 2018; Needham et al., 2021; Needham et al., 2022; Pascucci et al., 2020). Furthermore, our previous study has shown an increase in serum *p*CS levels of in *in utero* VPA-exposed male mice (Zheng et al., 2022). *p*CS has been detected in mouse brain tissue (Sun et al., 2020; Zgoda-Pols et al., 2011) and cerebrospinal fluid of parients with Parkinson's disease (Sankowski et al., 2020). In addition, 4EPS has also been demonstrated to be able to reach the brain in mice (Hsiao et al., 2013). In *in utero* VPA-exposed mice, the present study shows that hippocampal PTEN expression is decreased, which is in line with the previous finding that PTEN expression is decreased in hippocampus and cortex of in *in utero* VPA-exposed male mice (Mahmood et al., 2018). Decreased PTEN expression in brain might induce ASD-like behaviors, including impaired social interaction and increased repetitive behavior, which has also been demonstrated previously with PTEN-deficient mice (Lugo et al., 2014; Mahmood et al., 2018). However, it is not clear whether *p*CS or 4EPS derailes the neuroimmune responses of microglial cells *via* the induction of decreased PTEN in the hippocampus of *in utero* VPA-exposed male mice. This study showed that both *p*CS and 4EPS attenuated PTEN expression in BV2 micorglial cells constitutively and during LPS stimulation, indicating that these two ASD-associated bacterial derivates might be able to decrease PTEN expression directly in brain.

Next, we studied whether PTEN plays a role in the bacteria-derived metabolite-induced dysfunction of microglial cells *in vitro*. Both *p*CS and 4EPS attenuate constitutive and LPS-induced TNF-α and IL-6 release by BV2 microglial cells, which is supported by the finding that *p*CS attenuates LPS-induced inflammation in macrophages (Murakami et al., 2014; Shiba et al., 2016). However, PTEN inhibition did not affect the release of these cytokines in microglial cells, indicating that the *p*CS- and 4EPS-induced decreased PTEN expression does not play a role in the inhibitory effects of *p*CS and 4EPS on TNF-α and IL-6 release of by microglial cells. Interestingly, the present study showed that 4EPS, but not *p*CS, significantly increased constitutive COX-2 expression in microglial cells indicative for prostaglandin-associated inflammatory response. In contrast, COX-2 deficient mice show ASD pathogenesis and ASD-related behaviors (Kissoondoyal et al., 2021; Rai-Bhogal et al., 2018; Wong et al., 2019). The possible role of increased COX-2 expression triggered by 4EPS in microglial cells in the context of ASD remains to be investigated. Microglial phagocytosis is necessary to control synaptic function and brain development *via* regulating synaptic pruning and neuro-immune response (Irfan et al., 2022; Lenz and Nelson, 2018). In the present study, we found that neither 4EPS nor PTEN inhibition affected BV2 microglial phagocytosis activity. PTEN deficient mice show upregulated neuroinflammation and microglial phagocytosis (Sarn et al., 2021a; Sarn et al., 2021b). In contrast, it has also been reported that PTEN inhibition or knockdown attenuates neuroinflammation in mice (Pan et al., 2022; Shen et al., 2021). This study reports that PTEN did not play a role in ASD-associated bacterial metabolite-induced derailed immune and phagocytosis response of microglial cells. Additionally, PTEN is essential to maintain neuronal growth, synaptic function and brain connectivity (Skelton et al., 2019; Spina Nagy et al., 2021). Therefore, although beyond the scope of the present study, the role of the reduced PTEN expression observed in the brain of *in utero* VPA-exposed male mice, in the derailed neuronal network development and function remains to be further investigated.

In summary, this study demonstrated that both *p*CS and 4EPS decreased PTEN expression directly in microglial cells, which mirrors the decreased PTEN expression observed in the hippocampus of *in utero* VPA-exposed male mice. The current findings indicate that *p*CS and 4EPS-induced down-regulated PTEN does not play a role in ASD-associated neuroinflammation in the brain. Future studies are warranted in order to investigate how these two bacteria-derived metabolites affect neuronal synaptic function *in vitro* primary neurons and in *in vivo* ASD murine models with a focus on PTEN. Besides, It would be interesting that future experiments investigate whether *p*-cresol and 4-ethylphenol treatment can affect intestinal permeability in colonic epithelial cells and mice with a focus on PTEN. In addition, future studies colonizing mice with *p*-cresol and 4-ethylphenol producing bacteria would be promising approach to investigate their role in ASD-associated detrimental symptoms.

## Funding

This research was funded by the China Scholarship Council (CSC, Grant No. 201706210077 to YZ), and funded by European Commission Horizon 2020 (call H2020-SC1-BHC-03-2018), GEMMA project, Grant Agreement ID825033, www.gemma-project.eu.

## CRediT authorship contribution statement

Conceptualization—YZ, PPP, ADK; supervision—PPP, ADK, JG; investigation and data collection—YZ, NP, CVH; data analysis—YZ; writing—original draft preparation: YZ; writing—review and editing: YZ, NP, CVH, PPP, JG, ADK. All authors have read and agreed to the published version of the manuscript.

## Declaration of competing interest

All authors have seen and approved the final version of the manuscript being submitted. Johan Garssen is a part time employee at Danone Nutricia Research, Utrecht, The Netherlands. All other authors declare that the research was conducted in the absence of any commercial or financial relationships that could be construed as a potential conflict of interest.

## Data availability

Data will be made available on request.

## Acknowledgement

We would like to thank Prof. Dr. Ulrich L.M. Eisel for kindly donating mouse BV2 microglial cells.

## Appendix A. Supplementary data

Supplementary data to this article can be found online at https://doi.org/10.1016/j.mcn.2022.103805.

## References


Aïd, S., Bosetti, F., 2011. Targeting cyclooxygenases-1 and -2 in neuroinflammation: therapeutic implications. Biochimie 93, 46–51.

Avallone, R., Lucchi, C., Puja, G., Codeluppi, A., Filaferro, M., Vitale, G., Rustichelli, C., Biagini, G., 2020. BV-2 microglial cells respond to rotenone toxic insult by modifying pregnenolone, 5α-dihydroprogesterone and pregnanolone levels. Cells 9.

Babinská, K., Tomova, A., Celušáková, H., Babková, J., Repiská, G., Kubranská, A., Filčíková, D., Siklenková, L., Ostatníková, D., 2017. Fecal calprotectin levels correlate with main domains of the autism diagnostic interview-revised (ADI-R) in a sample of individuals with autism spectrum disorders from Slovakia. Physiol. Res. 66, S517–s522.

Bao, Y., Zhu, Y., He, G., Ni, H., Liu, C., Ma, L., Zhang, L., Shi, D., 2019. Dexmedetomidine attenuates neuroinflammation in LPS-stimulated BV2 microglia cells through upregulation of miR-340. Drug Des. Devel. Ther. 13, 3465–3475.

Bermudez-Martin, P., Becker, J.A.J., Caramello, N., Fernandez, S.P., Costa-Campos, R., Canaguier, J., Barbosa, S., Martinez-Gili, L., Myridakis, A., Dumas, M.E., Bruneau, A., Cherbuy, C., Langella, P., Callebert, J., Launay, J.M., Chabry, J., Barik, J., Le Merrer, J., Glaichenhaus, N., Davidovic, L., 2021. The microbial metabolite p-cresol induces autistic-like behaviors in mice by remodeling the gut microbiota. Microbiome 9, 157.

Bocchini, V., Mazzolla, R., Barluzzi, R., Blasi, E., Sick, P., Kettenmann, H., 1992. An immortalized cell line expresses properties of activated microglial cells. J. Neurosci. Res. 31, 616–621.

Brummer, T., Pigoni, M., Rossello, A., Wang, H., Noy, P.J., Tomlinson, M.G., Blobel, C.P., Lichtenthaler, S.F., 2018. The metalloprotease ADAM10 (a disintegrin and metalloprotease 10) undergoes rapid, postlysis autocatalytic degradation. FASEB J. 32, 3560–3573.

Busch, R.M., Srivastava, S., Hogue, O., Frazier, T.W., Klaas, P., Hardan, A., Martinez-Agosto, J.A., Sahin, M., Eng, C., 2019. Neurobehavioral phenotype of autism spectrum disorder associated with germline heterozygous mutations in PTEN. Transl. Psychiatry 9, 253.

Dalton, N., Chandler, S., Turner, C., Charman, T., Pickles, A., Loucas, T., Simonoff, E., Sullivan, P., Baird, G., 2014. Gut permeability in autism spectrum disorders. Autism Res. 7, 305–313.

de Theije, C.G., Koelink, P.J., Korte-Bouws, G.A., Lopes da Silva, S., Korte, S.M., Olivier, B., Garssen, J., Kraneveld, A.D., 2014. Intestinal inflammation in a murine model of autism spectrum disorders. Brain Behav. Immun. 37, 240–247.

Fombonne, E., MacFarlane, H., Salem, A.C., 2021. Epidemiological surveys of ASD: advances and remaining challenges. J. Autism Dev. Disord. 51, 4271–4290.

Frank, C.F., Hostetter, M.K., 2007. Cleavage of E-cadherin: a mechanism for disruption of the intestinal epithelial barrier by Candida albicans. Transl. Res. 149, 211–222.

Gabriele, S., Sacco, R., Cerullo, S., Neri, C., Urbani, A., Tripi, G., Malvy, J., Barthelemy, C., Bonnet-Brihault, F., Persico, A.M., 2014. Urinary p-cresol is elevated in young french children with autism spectrum disorder: a replication study. Biomarkers 19, 463–470.

Genovese, A., Butler, M.G., 2020. Clinical assessment, genetics, and treatment approaches in autism spectrum disorder (ASD). Int. J. Mol. Sci. 21.

Glynne, P.A., Darling, K.E., Picot, J., Evans, T.J., 2002. Epithelial inducible nitric-oxide synthase is an apical EBP50-binding protein that directs vectorial nitric oxide output. J. Biol. Chem. 277, 33132–33138.

Golden, J., Illingworth, L., Kavarian, P., Escobar, O., Delaplain, P., Isani, M., Wang, J., Lim, J., Bowling, J., Bell, B., Gayer, C.P., Grishin, A., Ford, H.R., 2020. EP2 receptor blockade attenuates COX-2 upregulation during intestinal inflammation. Shock (Augusta, Ga.) 54, 394–401.

Günaydin, C., Çelik, Z.B., Bilge, S.S., Avci, B., Kara, N., 2021. SAHA attenuates rotenone-induced toxicity in primary microglia and HT-22 cells. Toxicol. Ind. Health 37, 23–33.

Han, X., Fink, M.P., Yang, R., Delude, R.L., 2004. Increased iNOS activity is essential for intestinal epithelial tight junction dysfunction in endotoxemic mice. Shock (Augusta, Ga.) 21, 261–270.

Hsiao, E.Y., McBride, S.W., Hsien, S., Sharon, G., Hyde, E.R., McCue, T., Codelli, J.A., Chow, J., Reisman, S.E., Petrosino, J.F., Patterson, P.H., Mazmanian, S.K., 2013. Microbiota modulate behavioral and physiological abnormalities associated with neurodevelopmental disorders. Cell 155, 1451–1463.

Irfan, M., Evonuk, K.S., DeSilva, T.M., 2022. Microglia phagocytose oligodendrocyte progenitor cells and synapses during early postnatal development: implications for white versus gray matter maturation. FEBS J. 289 (8), 2110–2127.

Kang, D.W., Adams, J.B., Gregory, A.C., Borody, T., Chittick, L., Fasano, A., Khoruts, A., Geis, E., Maldonado, J., McDonough-Means, S., Pollard, E.L., Roux, S., Sadowsky, M. J., Lipson, K.S., Sullivan, M.B., Caporaso, J.G., Krajmalnik-Brown, R., 2017. Microbiota transfer therapy alters gut ecosystem and improves gastrointestinal and autism symptoms: an open-label study. Microbiome 5, 10.

Kang, D.W., Ilhan, Z.E., Isern, N.G., Hoyt, D.W., Howsmon, D.P., Shaffer, M., Lozupone, C.A., Hahn, J., Adams, J.B., Krajmalnik-Brown, R., 2018. Differences in fecal microbial metabolites and microbiota of children with autism spectrum disorders. Anaerobe 49, 121–131.

Kang, D.W., Adams, J.B., Vargason, T., Santiago, M., Hahn, J., Krajmalnik-Brown, R., 2020. Distinct fecal and plasma metabolites in children with autism spectrum disorders and their modulation after microbiota transfer therapy. mSphere 5.

Kissoondoyal, A., Rai-Bhogal, R., Crawford, D.A., 2021. Abnormal dendritic morphology in the cerebellum of cyclooxygenase-2(-) knockin mice. Eur. J. Neurosci. 54, 6355–6373.

Kwon, C.H., Luikart, B.W., Powell, C.M., Zhou, J., Matheny, S.A., Zhang, W., Li, Y., Baker, S.J., Parada, L.F., 2006. Pten regulates neuronal arborization and social interaction in mice. Neuron 50, 377–388.

Lenz, K.M., Nelson, L.H., 2018. Microglia and beyond: innate immune cells as regulators of brain development and behavioral function. Front. Immunol. 9, 698.

Lord, C., Elsabbagh, M., Baird, G., Veenstra-Vanderweele, J., 2018. Autism spectrum disorder. Lancet (London, England) 392, 508–520.

Lugo, J.N., Smith, G.D., Arbuckle, E.P., White, J., Holley, A.J., Floruta, C.M., Ahmed, N., Gomez, M.C., Okonkwo, O., 2014. Deletion of PTEN produces autism-like behavioral deficits and alterations in synaptic proteins. Front. Mol. Neurosci. 7, 27.

Mahmood, U., Ahn, S., Yang, E.J., Choi, M., Kim, H., Regan, P., Cho, K., Kim, H.S., 2018. Dendritic spine anomalies and PTEN alterations in a mouse model of VPA-induced autism spectrum disorder. Pharmacol. Res. 128, 110–121.

Mak, L.H., Vilar, R., Woscholski, R., 2010. Characterisation of the PTEN inhibitor VO-OHpic. J. Chem. Biol. 3, 157–163.

Murakami, Y., Kawata, A., Ito, S., Katayama, T., Fujisawa, S., 2014. Inhibitory effects of p-cresol and p-hydroxy anisole dimers on expression of the cyclooxygenase-2 gene and lipopolysaccharide-stimulated activation of nuclear factor-κB in RAW264.7 cells. In Vivo (Athens, Greece) 28, 719–725.

Nakazawa, H., Chang, K., Shinozaki, S., Yasukawa, T., Ishimaru, K., Yasuhara, S., Yu, Y. M., Martyn, J.A., Tompkins, R.G., Shimokado, K., Kaneki, M., 2017. iNOS as a driver of inflammation and apoptosis in mouse skeletal muscle after burn injury: possible involvement of Sirt1 S-nitrosylation-mediated acetylation of p65 NF-κB and p53. PloS one 12, e0170391.

Nam, H.Y., Nam, J.H., Yoon, G., Lee, J.Y., Nam, Y., Kang, H.J., Cho, H.J., Kim, J., Hoe, H. S., 2018. Ibrutinib suppresses LPS-induced neuroinflammatory responses in BV2 microglial cells and wild-type mice. J. Neuroinflamm. 15, 271.

Needham, B.D., Adame, M.D., Serena, G., Rose, D.R., Preston, G.M., Conrad, M.C., Campbell, A.S., Donabedian, D.H., Fasano, A., Ashwood, P., Mazmanian, S.K., 2021. Plasma and fecal metabolite profiles in autism spectrum disorder. Biol. Psychiatry 89, 451–462.

Needham, B.D., Funabashi, M., Adame, M.D., Wang, Z., Boktor, J.C., Haney, J., Wu, W.L., Rabut, C., Ladinsky, M.S., Hwang, S.J., Guo, Y., Zhu, Q., Griffiths, J.A., Knight, R., Bjorkman, P.J., Shapiro, M.G., Geschwind, D.H., Holschneider, D.P., Fischbach, M. A., Mazmanian, S.K., 2022. A gut-derived metabolite alters brain activity and anxiety behaviour in mice. Nature 602, 647–653.

Pan, R., Xie, Y., Fang, W., Liu, Y., Zhang, Y., 2022. USP20 mitigates ischemic stroke in mice by suppressing neuroinflammation and neuron death via regulating PTEN signal. Int. Immunopharmacol. 103, 107840.

Pascucci, T., Colamartino, M., Fiori, E., Sacco, R., Coviello, A., Ventura, R., Puglisi-Allegra, S., Turriziani, L., Persico, A.M., 2020. P-cresol alters brain dopamine metabolism and exacerbates autism-like behaviors in the BTBR mouse. Brain Sci. 10.

Persico, A.M., Napolioni, V., 2013. Urinary p-cresol in autism spectrum disorder. Neurotoxicol. Teratol. 36, 82–90.

Pigoni, M., Hsia, H.E., Hartmann, J., Rudan Njavro, J., Shmueli, M.D., Müller, S.A., Güner, G., Tüshaus, J., Kuhn, P.H., Kumar, R., Gao, P., Tran, M.L., Ramazanov, B., Blank, B., Hipgrave Ederveen, A.L., Von Blume, J., Mulle, C., Gunnersen, J.M., Wuhrer, M., Rammes, G., Busche, M.A., Koeglsperger, T., Lichtenthaler, S.F., 2020. Seizure protein 6 controls glycosylation and trafficking of kainate receptor subunits GluK2 and GluK3. EMBO J. 39, e103457.

Rai-Bhogal, R., Ahmad, E., Li, H., Crawford, D.A., 2018. Microarray analysis of gene expression in the cyclooxygenase knockout mice - a connection to autism spectrum disorder. Eur. J. Neurosci. 47, 750–766.

Ramakrishna, B.S., Roberts-Thomson, I.C., Pannall, P.R., Roediger, W.E., 1991. Impaired sulphation of phenol by the colonic mucosa in quiescent and active ulcerative colitis. Gut 32, 46–49.

Ristori, M.V., Quagliariello, A., Reddel, S., Ianiro, G., Vicari, S., Gasbarrini, A., Putignani, L., 2019. Autism, gastrointestinal symptoms and modulation of gut microbiota by nutritional interventions. Nutrients 11.

Rong, Y., Kiang, T.K.L., 2021. Characterization of human sulfotransferases catalyzing the formation of p-cresol sulfate and identification of mefenamic acid as a potent metabolism inhibitor and potential therapeutic agent for detoxification. Toxicol. Appl. Pharmacol. 425, 115553.

Salim, S., Banu, A., Alwa, A., Gowda, S.B.M., Mohammad, F., 2021. The gut-microbiota-brain axis in autism: what drosophila models can offer? J. Neurodev. Disord. 13, 37.

Sankowski, B., Księżarczyk, K., Raćkowska, E., Szlufik, S., Koziorowski, D., Giebułtowicz, J., 2020. Higher cerebrospinal fluid to plasma ratio of p-cresol sulfate and indoxyl sulfate in patients with Parkinson's disease. Clin. Chim. Acta 501, 165–173.

Sarn, N., Jaini, R., Thacker, S., Lee, H., Dutta, R., Eng, C., 2021a. Cytoplasmic-predominant Pten increases microglial activation and synaptic pruning in a murine model with autism-like phenotype. Mol. Psychiatry 26, 1458–1471.

Sarn, N., Thacker, S., Lee, H., Eng, C., 2021b. Germline nuclear-predominant Pten murine model exhibits impaired social and perseverative behavior, microglial activation, and increased oxytocinergic activity. Mol. Autism. 12, 41.

Seike, S., Takehara, M., Takagishi, T., Miyamoto, K., Kobayashi, K., Nagahama, M., 2018. Delta-toxin from Clostridium perfringens perturbs intestinal epithelial barrier function in Caco-2 cell monolayers. Biochim. Biophys. Acta Biomembr. 1860, 428–433.

Seike, S., Takehara, M., Kobayashi, K., Nagahama, M., 2019. Clostridium perfringens Delta-toxin damages the mouse small intestine. Toxins 11.

Shen, Y., Chen, L., Zhang, Y., Du, J., Hu, J., Bao, H., Xing, Y., Si, Y., 2021. Phosphatase and tensin homolog deleted on chromosome ten knockdown attenuates cognitive deficits by inhibiting neuroinflammation in a mouse model of perioperative neurocognitive disorder. Neuroscience 468, 199–210.

Shiba, T., Makino, I., Kawakami, K., Kato, I., Kobayashi, T., Kaneko, K., 2016. P-cresyl sulfate suppresses lipopolysaccharide-induced anti-bacterial immune responses in murine macrophages in vitro. Toxicol. Lett. 245, 24–30.

Skelton, P.D., Frazel, P.W., Lee, D., Suh, H., Luikart, B.W., 2019. Pten loss results in inappropriate excitatory connectivity. Mol. Psychiatry 24, 1627–1640.
Sonar, S.A., Lal, G., 2019. The iNOS activity during an immune response controls the CNS pathology in experimental autoimmune encephalomyelitis. Front. Immunol. 10, 710.
Spina Nagy, G., Kawamoto, E.M., Bridi, J.C., 2021. The role of PTEN signaling in synaptic function: implications in autism spectrum disorder. Neurosci. Lett. 759, 136015.
Stewart Campbell, A., Needham, B.D., Meyer, C.R., Tan, J., Conrad, M., Preston, G.M., Bolognani, F., Rao, S.G., Heussler, H., Griffith, R., Guastella, A.J., Janes, A.C., Frederick, B., Donabedian, D.H., Mazmanian, S.K., 2022. Safety and target engagement of an oral small-molecule sequestrant in adolescents with autism spectrum disorder: an open-label phase 1b/2a trial. Nat. Med. 28, 528–534.
Sun, C.Y., Li, J.R., Wang, Y.Y., Lin, S.Y., Ou, Y.C., Lin, C.J., Wang, J.D., Liao, S.L., Chen, C.J., 2020. p-Cresol sulfate caused behavior disorders and neurodegeneration in mice with unilateral nephrectomy involving oxidative stress and neuroinflammation. International journal of molecular sciences 21.
Terciolo, C., Dobric, A., Ouaissi, M., Siret, C., Breuzard, G., Silvy, F., Marchiori, B., Germain, S., Bonier, R., Hama, A., Owens, R., Lombardo, D., Rigot, V., André, F., 2017. Saccharomyces boulardii CNCM I-745 restores intestinal barrier integrity by regulation of E-cadherin recycling. J. Crohns Colitis 11, 999–1010.
Vanholder, R., Meert, N., Schepers, E., Glorieux, G., Argiles, A., Brunet, P., Cohen, G., Drüeke, T., Mischak, H., Spasovski, G., Massy, Z., Jankowski, J., 2007. Review on uraemic solutes II–variability in reported concentrations: causes and consequences. Nephrol. Dial. Transplant. 22, 3115–3121.
Velenosi, T.J., Hennop, A., Feere, D.A., Tieu, A., Kucey, A.S., Kyriacou, P., McCuaig, L.E., Nevison, S.E., Kerr, M.A., Urquhart, B.L., 2016. Untargeted plasma and tissue metabolomics in rats with chronic kidney disease given AST-120. Sci. Rep. 6, 22526.
Walker, S.J., Langefeld, C.D., Zimmerman, K., Schwartz, M.Z., Krigsman, A., 2019. A molecular biomarker for prediction of clinical outcome in children with ASD, constipation, and intestinal inflammation. Sci. Rep. 9, 5987.
Wang, D., Dubois, R.N., 2010. The role of COX-2 in intestinal inflammation and colorectal cancer. Oncogene 29, 781–788.
Wang, J., Zheng, B., Zhou, D., Xing, J., Li, H., Li, J., Zhang, Z., Zhang, B., Li, P., 2020. Supplementation of diet with different n-3/n-6 PUFA ratios ameliorates autistic behavior, reduces serotonin, and improves intestinal barrier impairments in a valproic acid rat model of autism. Front. Psych. 11, 552345.
Wang, L., Yu, Y.M., Zhang, Y.Q., Zhang, J., Lu, N., Liu, N., 2018. Hydrogen breath test to detect small intestinal bacterial overgrowth: a prevalence case-control study in autism. Eur. Child Adolesc. Psychiatry 27, 233–240.
Wei, S., Sun, J., Li, Y., Xu, K., Wang, M., Zhang, Y., 2022. Losartan attenuates atherosclerosis in uremic mice by regulating Treg/Th17 balance via mediating PTEN/PI3K/Akt pathway. Nephron 1–11.
Wong, C.T., Bestard-Lorigados, I., Crawford, D.A., 2019. Autism-related behaviors in the cyclooxygenase-2-deficient mouse model. Genes Brain Behav. 18, e12506.
Wu, X.X., Huang, X.L., Chen, R.R., Li, T., Ye, H.J., Xie, W., Huang, Z.M., Cao, G.Z., 2019. Paeoniflorin prevents intestinal barrier disruption and inhibits lipopolysaccharide (LPS)-induced inflammation in Caco-2 cell monolayers. Inflammation 42, 2215–2225.
Yang, L., Zhou, R., Tong, Y., Chen, P., Shen, Y., Miao, S., Liu, X., 2020. Neuroprotection by dihydrotestosterone in LPS-induced neuroinflammation. Neurobiol. Dis. 140, 104814.
Yehia, L., Seyfi, M., Niestroj, L.M., Padmanabhan, R., Ni, Y., Frazier, T.W., Lal, D., Eng, C., 2020. Copy number variation and clinical outcomes in patients with germline PTEN mutations. JAMA Netw. Open 3, e1920415.
Zamora, R., Vodovotz, Y., Billiar, T.R., 2000. Inducible nitric oxide synthase and inflammatory diseases. Molecular medicine (Cambridge, Mass.) 6, 347–373.
Zgoda-Pols, J.R., Chowdhury, S., Wirth, M., Milburn, M.V., Alexander, D.C., Alton, K.B., 2011. Metabolomics analysis reveals elevation of 3-indoxyl sulfate in plasma and brain during chemically-induced acute kidney injury in mice: investigation of nicotinic acid receptor agonists. Toxicol. Appl. Pharmacol. 255, 48–56.
Zheng, Y., Bek, M.K., Prince, N.Z., Peralta Marzal, L.N., Garssen, J., Perez Pardo, P., Kraneveld, A.D., 2021. The role of bacterial-derived aromatic amino acids metabolites relevant in autism spectrum disorders: a comprehensive review. Front. Neurosci. 15, 738220.
Zheng, Y., Prince, N.Z., Peralta Marzal, L.N., Ahmed, S., Garssen, J., Perez Pardo, P., Kraneveld, A.D., 2022. The autism Spectrum disorder-associated bacterial metabolite p-cresol derails the neuroimmune response of microglial cells partially via reduction of ADAM17 and ADAM10. Int. J. Mol. Sci. 23, 11013.
Zou, R., Xu, F., Wang, Y., Duan, M., Guo, M., Zhang, Q., Zhao, H., Zheng, H., 2020. Changes in the gut microbiota of children with autism spectrum disorder. Autism Res. 13, 1614–1625.